Journal of the Mechanics and Physics of Solids 124 (2019) 143–158

Contents lists available at ScienceDirect

Journal of the Mechanics and Physics of Solids

journal homepage: www.elsevier.com/locate/jmps

# Delayed burst of a gel balloon

Jian Cheng[a], Zheng Jia[b,c,*], Hongyu Guo[d], Zhihong Nie[d], Teng Li[a,*]

[a] Department of Mechanical Engineering, University of Maryland, College Park, MD 20742, United States
[b] Department of Engineering Mechanics, Zhejiang University, Hangzhou 310027, China
[c] Key Laboratory of Soft Machines and Smart Devices of Zhejiang Province, Zhejiang University, Hangzhou 310027, China
[d] Department of Chemistry and Biochemistry, University of Maryland, College Park, MD 20742, United States

ARTICLE INFO

*Article history:*
Received 31 July 2018
Revised 3 October 2018
Accepted 10 October 2018
Available online 13 October 2018

ABSTRACT

When inflating a rubber balloon, it is commonly concluded that a sudden expansion in balloon size (i.e., the burst) occurs once the inner pressure reaches a critical threshold, the instantaneous burst pressure. Such burst phenomena are usually attributed to the snap-through instability. In this work, we demonstrate that when a hydrogel balloon is subject to a subcritical pressure lower than the instantaneous burst pressure, the hydrogel balloon may remain stable for a span of time, and then burst suddenly. We refer to such burst phenomena as the delayed burst of the gel balloon. When subject to such a subcritical inner pressure, a hydrogel balloon slowly and continuously absorbs solvent and swells. We find the instantaneous burst pressure of the hydrogel balloon to be a decreasing function of swelling ratio. The criterion for the onset of burst is that the swelling-related instantaneous burst pressure drops to the applied inner pressure. The delayed burst can, therefore, be attributed to the time needed for the hydrogel swelling to reduce the instantaneous burst pressure to the level of applied pressure. We further delineate a map indicating three distinct deformation modes of gel balloons, i.e., instantaneous burst, delayed burst, and steady deformation without burst (safe mode), in the parameter space of applied pressure and mechanical properties of the hydrogel. The delayed burst of a hydrogel balloon is counterintuitive and a crucial aspect in developing hydrogel-shell-based soft actuators and soft machines. The research findings may shed light on the understanding of the complex failure mechanisms of hydrogel actuators and also facilitate the design of hydrogel-based tissue delivery capsules.

© 2018 Published by Elsevier Ltd.

## 1. Introduction

Hollow thin-shell structures have found widespread applications from as small as nano-anodes in Li-ion batteries (Yao et al., 2011) to as large as radar domes and fuel tanks (Godoy, 2016). The past decade has witnessed a wealth of attentions paid to soft thin shells, which represent a paradigm shift in research interests from conventional rigid structures to deformable, inflatable, and multifunctional components. For instance, the use of soft polymeric thin shells has been embraced as a trending strategy for soft actuator and soft robot design: inflated either pneumatically or hydraulically, such a

* Corresponding author at: Department of Engineering Mechanics, Zhejiang University, Hangzhou 310027, China, and Department of Mechanical Engineering, University of Maryland, College Park, MD 20742, United States
*E-mail addresses:* zheng.jia@zju.edu.cn (Z. Jia), lit@umd.edu (T. Li).

https://doi.org/10.1016/j.jmps.2018.10.010
0022-5096/© 2018 Published by Elsevier Ltd.

strategy provides a promising avenue for agile and swift actuation. By controlling the pressurization of each individual joint in concert with the others, the actuators are able to achieve complex motions, such as walking (Ainla et al., 2017; Nemiroski et al., 2017; Shepherd et al., 2011), jumping (Bartlett et al., 2015), swimming (Marchese et al., 2014; Yuk et al., 2017), and gripping (Acome et al., 2018). For example, Wehner et al. successfully prototyped a soft octopus-like robot and controlled its motion via an embedded microfluidic system (Wehner et al., 2016); Acome et al. designed a soft gripper driven by the localized inflation of a hollow structure by electrostatically directing the motion of liquid dielectrics (Acome et al., 2018); Kim et al. demonstrated a multifunctional inflatable catheter as a surgical tool that delivers therapy and diagnosis to desired local lesions (Kim et al., 2011). Despite successful applications of soft polymeric thin-shell structures in soft actuators and medical devices, their applications in biomedical engineering and tissue engineering are often hindered by poor biocompatibility arising from the physical dissimilarity between polymeric materials and living tissues.

Hydrogels are composed of considerable amount of water and a polymer network. This unique combination provides biocompatibility, permeability, and deformability. For this reason, hydrogel thin-shell structures such as hydrogel capsules have emerged in a myriad of biomedical applications such as *in vitro* 3D tissue culture (Lu et al., 2015; Mytnyk et al., 2017a; Song et al., 2015; Zhao et al., 2014), biomedical sensors (Alessandri et al., 2013), cell-based therapy development (Lima et al., 2013; Olabisi et al., 2010; Wang and Wang, 2014), drug delivery (Luo et al., 2014), and bio-mimicking structures (Yoshida and Onoe, 2017). Alessandri et al. described a method to culture tumor cellular aggregations encapsulated in cross-linked alginate hydrogel shells. By monitoring the expansion or even burst of the hollow spherical hydrogel shells, the growth of tumor cells under mechanical confinement can be directly investigated (Alessandri et al., 2013). In addition, for applications such as drug release (Li and Mooney, 2016) and cell therapy (Griffin et al., 2015), the burst and degradation of the hydrogel capsule play a pivotal role. That is, the burst event has to precisely concur with the drug's arrival at the delivery target or the tissue's full development. A premature release only results in an unsuccessful delivery of underdeveloped tissues, whereas a late burst may cause adverse reactions (Alijotas-Reig et al., 2013; Griffin et al., 2015). Therefore, understanding the deformation and burst mechanism is the key to successful applications of hydrogel thin-shell structures in biomedical and tissue engineering.

Inflation and burst of an elastomeric thin-walled structure have long been a focal topic of solid mechanics. One of the earliest accounts of the inflation of a rubber balloon is predicted analytically by Feodos'ev (1968). This pioneering work was followed by others with their main attention devoted to the inflation response of hyperelastic materials with different constitutive assumptions (Alexander, 1971; Bogen and McMahon, 1979; Merritt and Weinhaus, 1978; Needleman, 1977) and of different geometries (Chen and Healey, 1991; deBotton et al., 2013). According to these classical notes, it is both observed experimentally and concluded theoretically that, when inflating a rubber balloon, a sudden expansion in balloon size (i.e., the burst) occurs once the inner pressure reaches a critical threshold, the instantaneous burst pressure. Such burst phenomena are commonly attributed to the snap-through instability. Based on these understandings, most recent research interests are also directed to harness such snap-through instability to our benefit, such as achieving enhanced actuation performances of soft actuators (Li et al., 2013; Overvelde et al., 2015), or to investigate the highly enriched deformation bifurcations of electrically active soft materials due to instability (Lu et al., 2015; Wang et al., 2017).

Despite extensive studies on elastomeric thin-walled structures, the instability of hollow hydrogel structures is far from being well understood. Wang and Cai investigated drying-induced growth of inner cavity in confined hollow spherical hydrogels Wang and Cai, 2015a), however, in that study, the inflation of the hydrogels is restricted by a rigid confinement at its outer surface. Alessandri et al. experimentally observed growth-induced bursts of spherical hydrogel capsules in the culture of tumor tissue, however, a quantitative mechanistic understanding of the burst of hydrogel capsules remains elusive (Alessandri et al., 2013). To address these unsolved issues, a systematic study of inflation and burst of hollow thin-walled hydrogel structures should be carried out. Most recently, Zamani and Pence investigated the swelling-induced burst of a swellable Mooney–Rivlin spherical shell (Zamani and Pence, 2017): the pressure-expansion response was simply studied by assigning an increasing swelling factor to the elastic shell; However, some key questions still remain unclear in their study: (1) What is the underlying physics bestowing the swellable behavior of the hyperelastic network? (2) Will the balloon shell further swell under inner pressurization? (3) If the further swelling indeed occurs, what serves as the driving force and to what extent the balloon shell will swell? In the present paper, we will directly answer these open questions.

As aforementioned, hydrogels intrinsically differ from elastomers and polymers. In hydrogel, the polymer chains are interacting with water molecules by weak intermolecular forces. When a hydrogel is in contact with an aqueous environment and subject to mechanical loads and confinements, water migrates in and out of the hydrogel to accommodate the applied loads and boundary conditions. Therefore, the deformation behavior and the failure of a hydrogel structure also deviate from its water-free elastomeric counterparts. For example, when a hydrogel sample containing a pre-crack is subject to a static load less than the critical load for instantaneous fracture, the pre-crack initially remains virtually stationary for some time, followed by sudden and rapid propagation, causing catastrophic fracture. Such a fracture mode of hydrogel is referred to as delayed fracture (Bonn et al., 1998; Mao and Anand, 2018; Tang et al., 2017; Wang and Hong, 2012a), which is usually attributed to viscoelasticity stemming from the mechano-chemical reaction in stressed molecular chains (Chaudhury, 1999; Skrzeszewska et al., 2010), dissociation of physical crosslinks (Baumberger et al., 2006; Lindström et al., 2012), and migration of water molecules (Wang and Hong, 2012a). Nonetheless, existing investigations into the delayed failures of hydrogels are primarily limited to their fracture.

Herein, we unveil the delayed burst of hollow spherical thin-walled hydrogel structures (i.e., hydrogel balloons), a failure mode that has not as yet investigated. Under an interior pressure, a hydrogel balloon gradually and continuously absorbs water and swells. This fact leads to the anomalous delayed burst behavior of a hydrogel balloon: when subject to a subcritical

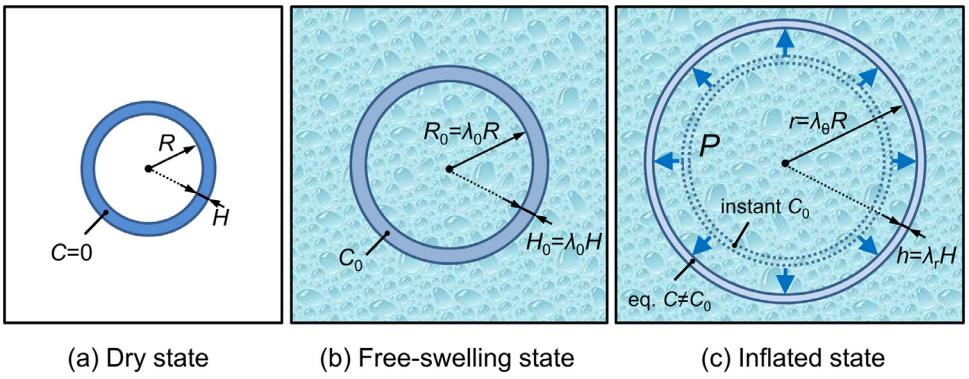


**Fig. 1.** Schematic of the inflation process of a hydrogel balloon. (a) The dry state of a hydrogel balloon with its radius being $R$ and thickness $H$, where $H \ll R$. (b) The free-swelling equilibrium state of the hydrogel balloon in water. (c) The inflated states of the balloon under an inner pressure $P$. Dashed-line shell: instant deformation under a fast pressurization ($t_p \ll t_{eq}$); solid-line shell: long-term final deformation of the hydrogel balloon due to a fast inflation ($t_p \ll t_{eq}$) or quasi-equilibrium deformation during a slow inflation ($t_p \gg t_{eq}$).

pressure less than the instantaneous burst threshold, the hydrogel balloon remains stable for a span of time, slowly grows and swells, then expands suddenly in size until bursts to fracture. Delayed burst is counterintuitive as it is triggered by a load below the critical threshold for instantaneous fracture. Such a failure phenomenon is also more detrimental than instantaneous burst, given its latent nature. Even worse, delayed burst may complicate other failure mechanisms of a hydrogel balloon, such as delayed fracture (Wang and Hong, 2012a), structure buckling (Marthelot et al., 2017), and swelling induced wrinkling (Bertrand et al., 2016; Curatolo et al., 2017), especially in the presence of geometry imperfections (Lee et al., 2016) and material defects (Kundu and Crosby, 2009; Scherer and Smith, 1995; Wang and Cai, 2015a, b; Wang and Hong, 2012a). From the perspective of applications, whether it is on one end of the spectrum where the burst phenomenon is intended as a design feature to fulfill functions such as drug release and cell delivery, or on the opposite end where delayed burst is deemed as a failure mode of applications such as soft actuators, soft robots, and *in vitro* cell cultivation, an accurate mechanistic understanding of the delayed burst of hydrogel balloons is of vital importance.

The rest of this paper is organized as follows. In Section 2, we examine the long-term, hence equilibrium deformation behavior of a hydrogel balloon under interior pressurization at a constant load. The most intriguing finding is the balloon's propensity to imbibe more water molecules into its hydrogel shell, accompanying its expansion in size. Section 3 investigates the instantaneous response of a hydrogel balloon when subject to a rapidly supplied pressure. The findings in Sections 2 and 3 lead to a theoretical explanation of the delayed burst phenomenon of a hydrogel balloon in Section 4. In Section 5, we extend the study to the burst behavior of a hydrogel shell with a finite thickness.

## 2. The long-term response of a hydrogel balloon after fast pressurization

The inflation process of a hydrogel balloon is depicted in Fig. 1. In its completely dehydrated state (water concentration $C=0$), a spherical hydrogel shell (or a hydrogel balloon) has a radius of $R$ and a thickness of $H$, as shown in Fig. 1(a). In this section, we first consider a thin spherical balloon, namely $H \ll R$. When immersed in water, the hydrogel balloon swells uniformly to a stress-free state with a water concentration $C_0$ and an isotropic stretch ratio $\lambda_0$, such that the network equilibrates with the water surrounding in absence of mechanical load. With this stress-free stretch ratio $\lambda_0$, the radius expands to $R_0=\lambda_0 R$ and the thickness increases to $H_0=\lambda_0 H$ (Fig. 1(b)). In the next step, the balloon is inflated by applying an internal pressure $P$, accordingly, the radius further expands to $r$ and the thickness becomes $h$. Under an evenly distributed interior pressure, the inflated hydrogel balloon retains the spherical symmetry. Provided that the thickness of the balloon shell is much smaller than the overall size of the balloon, the variation over the thickness of both hoop stretch $\lambda_\theta$ and radial stretch $\lambda_r$ are negligible. Thus, $\lambda_\theta$ can be evaluated approximately at the inner surface; similarly, $\lambda_r$ can be estimated as the average over the entire thickness, namely

$$\lambda_\theta = \frac{r}{R},\ \lambda_r = \frac{h}{H} \tag{1}$$

where $\lambda_\theta$ and $\lambda_r$ represent the hoop and radial stretches with respect to the dry state, respectively.

The deformation of hydrogels in response to mechanical forces is time-dependent, resulting from the migration of water molecules. The time needed by the hydrogel balloon to reach an equilibrium via water diffusion, $t_{eq}$, approximately scales with $H_0^2/D$. Here $H_0$, the free-swelling shell thickness, constitutes the characteristic length; $D$ represents the diffusivity of water molecules transporting through the hydrogel. Another time scale relevant to the balloon inflation, the time of the pressurization procedure $t_p$, is defined as the time period as the inner pressure builds up from 0 to $P$. Depending on the comparison between $t_{eq}$ and $t_p$, the balloon exhibits disparate mechanical responses to the applied pressure. In the scenarios where pressurization occurs very fast, i.e., $t_p \ll t_{eq}$, the local water concentration inside the hydrogel remains at the same

level $C_0$ as the free-swelling state during the entire loading process, since the time of pressurization $t_p$ is too short for any water molecule to migrate. Immediately after the completion of a fast pressurization procedure (at $t=t_p$), the hydrogel balloon deforms to what we term the instantaneous inflated state, as sketched schematically by the dashed-lines in Fig. 1(c).

Considering the molecular incompressibility (Hong et al., 2009, 2008), the volume ratio $J$ can be related to the local water concentration $C$ through

$$J = 1 + \nu C \tag{2}$$

where $\nu$ is the volume per water molecule. This equation implies that in hydrogel both the polymeric network and the water molecules are incompressible. As a result, the volume of the hydrogel is a summation of the volume of these two constituents. Therefore, because of the unchanged water concentration $C$, the balloon's instantaneous response to a fast inflation is featured by a volume-conserving deformation, similar to the deformation of elastomeric materials, whose volume change is often negligible. Note that here the conserved volume refers to that of the hydrogel shell rather than the volume enclosed by the balloon; the enclosure volume will nevertheless increase as the balloon expands.

However, if the pressure is applied during a slow process ($t_p \gg t_{eq}$) that takes place incrementally and in a quasi-equilibrium manner, the inflation is accompanied with water transportation across the hydrogel network. According to the molecular incompressibility condition (Eq. (2)), with more water content uptake, the volume of the hydrogel shell increases by the volume of the water entering the polymeric network; and conversely, it decreases due to local water content loss. Therefore, the water concentration $C$ is subject to vary in these equilibrium deformations ($C \neq C_0$). While the pressure builds up, the water molecules also take time to migrate, allowing the deformation of the balloon to pass gradually through a series of quasi-equilibrium states. Moreover, for fast inflation ($t_p \ll t_{eq}$) if the applied pressure is maintained after the completion of loading, i.e., $P=$const for $t > t_p$, the hydrogel balloon also evolves towards a final equilibrium state, which is the long-term response to pressure $P$. Regardless the loading characteristics, given the same applied pressure, the equilibrium responses are essentially the same. The boundary of the equilibrium deformation state is defined by the solid shell in Fig. 1(c).

In this section, we focus our attention on the long-term/equilibrium deformation of a hydrogel balloon, while leave the instantaneous response to be studied in the next section. Following previous works (Hong et al., 2009, 2008), when immersed in a solvent reservoir with a constant chemical potential $\mu$, the free energy density of a hydrogel in the reference state can be expressed by

$$W = \frac{1}{2}NkT\left(\lambda_1^2+\lambda_2^2+\lambda_3^2-3-2\log J\right) - \frac{kT}{\nu}\left[(J-1)\log\left(\frac{J}{J-1}\right)+\frac{\chi}{J}\right] - \frac{\mu}{\nu}(J-1) \tag{3}$$

where $N$ is the number of polymer chains per unit volume in the dry state, $kT$ is the absolute temperature in unit of energy, $\lambda_i$ ($i=1, 2, 3$) denotes the principal stretches of the deformed state, $J=\lambda_1\lambda_2\lambda_3$ is the volume ratio and is related to the local water content through Eq. (2), and $\chi$ is the dimensionless Flory–Huggins parameter representing the enthalpy of mixing.

The principal component of the nominal stress and Cauchy stress can be calculated by

$$\frac{S_i}{kT/\nu} = \frac{\partial}{\partial\lambda_i}\left(\frac{W}{kT/\nu}\right) = N\nu\left(\lambda_i-\lambda_i^{-1}\right)+\lambda_i^{-1}\left[J\log\left(1-\frac{1}{J}\right)+1+\frac{\chi}{J}-\frac{\mu}{kT}J\right] \tag{4.1}$$

$$\frac{\sigma_i}{kT/\nu} = \frac{\lambda_i}{J}\frac{S_i}{kT/\nu} = \frac{N\nu}{J}\left(\lambda_i^2-1\right)+\left[\log\left(1-\frac{1}{J}\right)+\frac{1}{J}+\frac{\chi}{J^2}-\frac{\mu}{kT}\right] \tag{4.2}$$

In particular, relative to the dry polymer network, a freestanding hydrogel immersed in water swells with isotropic stretches $\lambda_1=\lambda_2=\lambda_3=\lambda_0$, where $\lambda_0$ denotes the isotropic free-swelling stretch. Since the free-swelling state is associated with a stress-free deformation, $\lambda_0$ can be determined by equating the Cauchy stress in the hydrogel to zero. Given the value of $N\nu$, the free-swelling ratio $\lambda_0$ can be expressed as follows:

$$N\nu\left(\lambda_0^{-1}-\lambda_0^{-3}\right)+\log\left(1-\lambda_0^{-3}\right)+\lambda_0^{-3}+\chi\lambda_0^{-6}-\mu/kT=0 \tag{5}$$

The dimensionless group $N\nu$ is identified as the shear modulus of the dry state polymer under infinitesimal strain.

When subjected to an evenly distributed interior pressure, a hydrogel balloon undergoes spherically symmetric deformation. Taking advantage of symmetry, we have hoop stretches $\lambda_1=\lambda_2=\lambda_\theta$, radial stretch $\lambda_3=\lambda_r$, and volume ratio $J=\lambda_\theta^2\lambda_r$. Plugging these relations into Eq. (4.1), the nominal hoop and radial stresses are

$$\frac{S_\theta}{kT/\nu} = N\nu\left(\lambda_\theta-\lambda_\theta^{-1}\right)+\lambda_\theta^{-1}\left[J\log\left(1-\frac{1}{J}\right)+1+\frac{\chi}{J}-\frac{\mu}{kT}J\right] \tag{6.1}$$

$$\frac{S_r}{kT/\nu} = N\nu\left(J\lambda_\theta^{-2}-J^{-1}\lambda_\theta^2\right)+J^{-1}\lambda_\theta^2\left[J\log\left(1-\frac{1}{J}\right)+1+\frac{\chi}{J}-\frac{\mu}{kT}J\right] \tag{6.2}$$

And the Cauchy stresses in the hoop and radial directions can be calculated by using Eq. (4.2) as

$$\frac{\sigma_\theta}{kT/\nu} = J^{-1}N\nu\left(\lambda_\theta^2-1\right)+\left[\log\left(1-\frac{1}{J}\right)+\frac{1}{J}+\frac{\chi}{J^2}-\frac{\mu}{kT}\right] \tag{7.1}$$

$$\frac{\sigma_r}{kT/\nu} = J^{-1}N\nu\left(\lambda_\theta^{-4}J^2-1\right)+\left[\log\left(1-\frac{1}{J}\right)+\frac{1}{J}+\frac{\chi}{J^2}-\frac{\mu}{kT}\right] \tag{7.2}$$

In the deformed configuration, the force balance in the radial direction gives

$$\frac{d\sigma_r}{d\rho}+2\frac{\sigma_r-\sigma_\theta}{\rho}=0\ (r\le\rho\le r+h) \tag{8}$$

where $\rho$ is the radius of a differential spherical layer in the deformed configuration. Consider that for a thin-walled hydrogel balloon with $H\ll R$, when inflated, the tensile stress in the hoop direction $\sigma_\theta$ is orders of magnitude greater than the compressive stress in the thickness direction $\sigma_r$. Therefore, the triaxial stress state in the balloon shell can be approximated by an equal-biaxial state, namely,

$$\sigma=\begin{bmatrix}\sigma_\theta & & \\ & \sigma_\theta & \\ & & \sigma_r\end{bmatrix}\approx\begin{bmatrix}\sigma_\theta & & \\ & \sigma_\theta & \\ & & 0\end{bmatrix} \tag{9}$$

Moreover, in a thin-walled hydrogel balloon, $\sigma_\theta$ barely varies over the thickness of the balloon shell. Although $\sigma_r$ varies from $-P$ to 0 through the thickness, its magnitude is trivial compared to the hoop stress $\sigma_\theta$. As a result, the value of $(\sigma_\theta-\sigma_r)/\rho$ in Eq. (8) can be treated as a constant over the entire thickness of the balloon shell. In the deformed coordinate, integrating Eq. (8) from the pressurized inner surface to the stress-free outer surface of the balloon

$$\int_{-P}^{0}d\sigma_r=2\int_{r}^{r+h}\frac{\sigma_\theta-\sigma_r}{\rho}d\rho \tag{10}$$

yields

$$\sigma_\theta-\sigma_r=\frac{Pr}{2h} \tag{11}$$

Substituting Eqs. (7.1) and (7.2) and the relations that $\lambda_\theta=r/R$ and $\lambda_r=h/H$ into Eq. (11) we can express the inflation pressure $P$ as a function of $J$ and $\lambda_\theta$

$$\frac{P}{kT/v}=\frac{2H}{R}Nv\cdot\left(\lambda_\theta^{-1}-\lambda_\theta^{-7}J^2\right) \tag{12}$$

By adopting an approximation of the equal-biaxial stress state, $\sigma_r$ vanishes, so that Eq. (6.2) gives

$$J^{-1}Nv\left(\lambda_\theta^{-4}J^2-1\right)+\left[\log\left(1-\frac{1}{J}\right)+\frac{1}{J}+\frac{\chi}{J^2}-\frac{\mu}{kT}\right]=0 \tag{13}$$

Combining Eqs. (12) and (13), we establish the mechanical behavior of the hydrogel balloon as a relation between the pressure $P$ and the equilibrium deformation state of the balloon ($J$ and $\lambda_\theta$). Given the thin-walled geometry of the balloon, we can further ignore the variation of $J$, $\lambda_\theta$, and $\lambda_r$ over the thickness. Therefore, the deformation is homogeneous throughout the balloon shell and can be completely set by two parameters $J$ and $\lambda_\theta$ (here $J$, $\lambda_r$, and $\lambda_\theta$ are not independent since $J=\lambda_r\lambda_\theta^2$). $\lambda_\theta=r/R$ indicates the size of the balloon: a larger $\lambda_\theta$ corresponds to a further inflated state, i.e., a larger balloon; while $J$ suggests the steady-state water concentration inside the balloon shell, a higher value of $J$ implies more water content is absorbed into the hydrogel network in the current equilibrium frame. When material properties and geometry parameters ($Nv$, $\chi$, $\mu$, and $H/R$) are specified, the equilibrium deformation state of the hydrogel balloon can be identified for any given inner pressure $P$ by solving Eqs. (12) and (13). Representative values of the dimensionless crosslinking density of a hydrogel $Nv$ may vary over $1\times10^{-4}\sim1\times10^{-1}$, and the Flory–Rehner interaction parameter $\chi$ typically ranges 0∼1.2 (Hong et al., 2009). In the numerical examples below, we will take values, $\chi=0.2$, $H/R=0.01$, and the chemical potential of the water reservoir $\mu=0$, unless otherwise mentioned.

For different values of $Nv$ (0.001, 0.003, 0.005, and 0.007), Fig. 2(a) plots the correlation among normalized pressure $Pv/kT$, volume strain $J$, and hoop stretch $\lambda_\theta$ as a family of three-dimensional curves, such that the equilibrium response of a hydrogel to applied pressure is readily spotted. Projecting these curves onto $J$-$\lambda_\theta$ plane, as shown in Fig. 2(b), $J$ is plotted as a function of $\lambda_\theta$. Starting from the free-swelling state (marked by the squares, for example), along the inflation process the expansion of the gel balloon is accompanied with a monotonic increase of $J$, indicating a spontaneous migration of water into the balloon shell as the balloon expands in size. This fact can be ascribed to the equal-biaxial tensile stress state in the hydrogel balloon (Fujine et al., 2015).

Fig. 2(c) shows the relation between the dimensionless internal pressure $Pv/kT$ and the normalized balloon size $r/R$. For example, when $Nv=0.001$ the inflation procedure starts at its free-swelling state $\lambda_0=3.21$. The pressure $Pv/kT$ required by an equilibrium state of the hydrogel balloon continues to increase until a maximum magnitude of $3.04\times10^{-6}$ is reached as the balloon expands to $r/R=5.00$. Thereafter, the pressure drops for further inflation, indicating the existence of a critical pressure $P_{cr}$ (dashed line) above which no equilibrium deformed states can be obtained. Any quasi-equilibrium inflation process with a pressure above $P_{cr}$ would lead to a continual and infinite growth in the balloon size, resulting in burst of the hydrogel balloon.

Moreover, the swelling also becomes infinite if the critical pressure is exceeded because of the simultaneous increasing of the swelling ratio and hoop stretch. It is concluded from Fig. 2(d) that when a pressure $P$ less than $P_{cr}$ is applied, the hydrogel swells and the volume ratio $J$ evolves to a corresponding equilibrium state which can be recognized on the lower half of the curve in Fig. 2(d), as illustrated by the arrow. For $P<P_{cr}$, the higher the applied pressure, the more the hydrogel

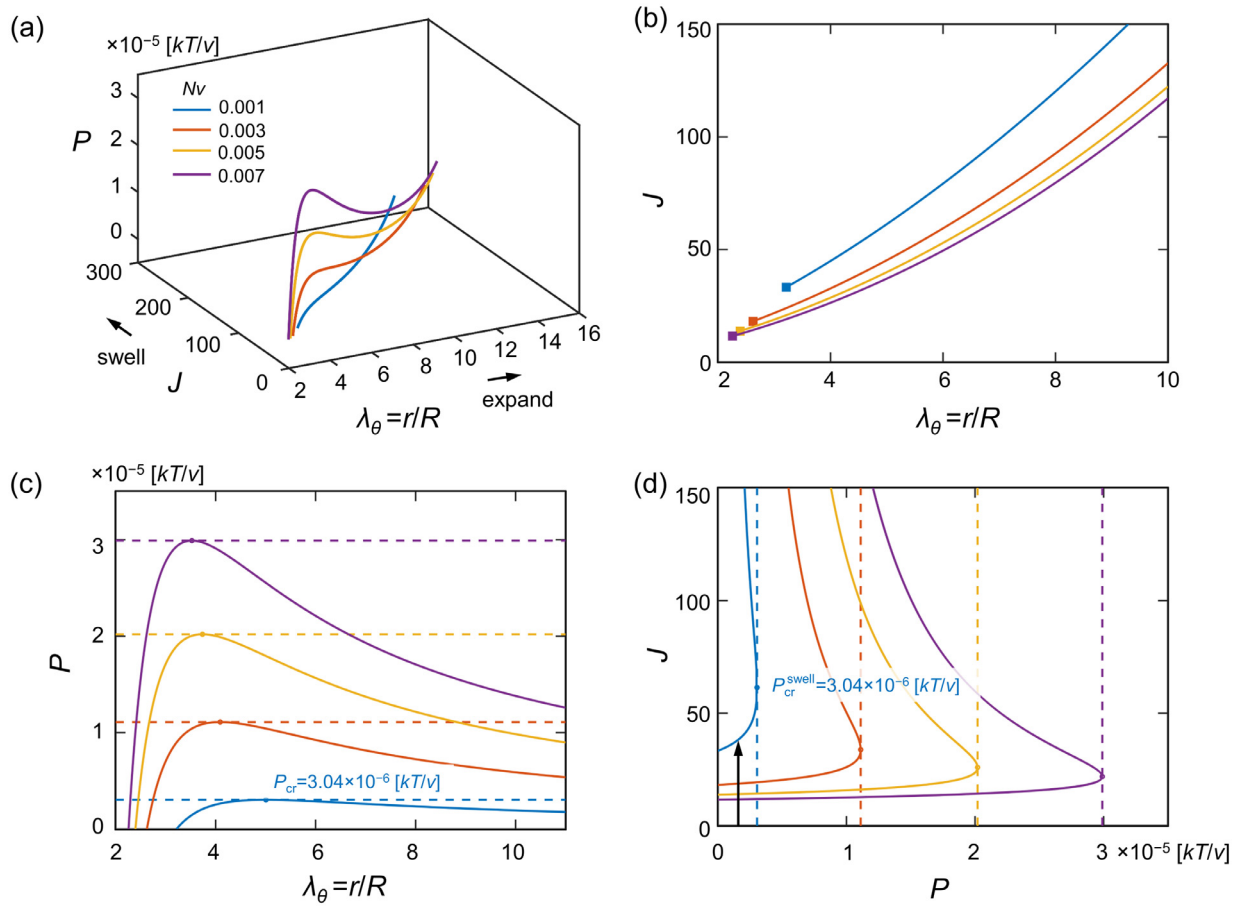


**Fig. 2.** Long-term equilibrium deformation of a hydrogel balloon. (a) Three-dimensional curves representing the relation between applied pressure $Pv/kT$ and the equilibrium deformations for hydrogel balloons with different $Nv$ values ($Nv = 0.001$, 0.003, 0.005, and 0.007). (b) $J$ as a function of $\lambda_\theta$; $J$ and $\lambda_\theta$ are volume strain and hoop stretch with respect to the dehydrated state. Curves start from the free-swelling states (labeled by the squares) for each hydrogel balloon. (c) Normalized pressure $Pv/kT$ as a function of $\lambda_\theta$. (d) Volume ratio $J$ as a function of applied pressure $Pv/kT$. In (c) and (d), the maximum pressure permitting the existence of equilibrium deformation and bounded swelling is marked by the dashed lines. The black arrow indicates an equilibrium final deformation when $P < P_{\mathrm{cr}}^{\mathrm{swell}}$.

swells in its final equilibrium state. In contrast, beyond $P_{\mathrm{cr}}$, the water absorption becomes unbounded due to the lack of equilibrium state. Water molecules will continuously migrate into the hydrogel. Therefore, the critical pressure $P_{\mathrm{cr}}$ for equilibrium deformation can be physically interpreted as a threshold for unbounded swelling $P_{\mathrm{cr}}^{\mathrm{swell}}$. Such an unbounded swelling will invoke anomalous inflation behavior of the hydrogel balloon, as to be discussed in the following sections.

## 3. The instantaneous response of a hydrogel balloon to fast inflation

As aforementioned, the pressurization time scale governs the mechanical responses of a hydrogel balloon. When an internal pressure is applied suddenly ($t_{\mathrm{p}} \ll t_{\mathrm{eq}}$), the instantaneous response of the balloon is characterized by a volume-conserving deformation, similar to that of elastomeric materials. In an effort to determine the instantaneous inflation behavior subject to fast inflation, we first consider a homogeneously swollen hydrogel balloon with an arbitrary water concentration $\hat{C}$ inside the balloon shell. Let us denote this swollen state of the gel balloon as state S($\hat{C}$), referring to its homogeneous water distribution. In state S($\hat{C}$), the corresponding isotropic swelling ratio can be calculated by

$$\hat{\lambda} = \left(1 + v\hat{C}\right)^{\frac{1}{3}} \tag{14}$$

Next, we think of a scenario where the boundaries of the balloon become impermeable so that solvent exchange between hydrogel balloon and the reservoir is prohibited. We take the hydrogel shell containing polymer chains and water content as the control volume. Under such an impermeable boundary condition, the balloon shell is therefore turned into a closed system with a constant water concentration remaining at $\hat{C}$. Any subsequent deformation of the hydrogel is thus incompressible and the volume ratio $\hat{J}$ remains fixed. The incompressibility constraint can be written as

$$J = \hat{J} = 1 + v\hat{C} = \hat{\lambda}^3 = \mathrm{const} \tag{15}$$

Given the fixed volume ratio, the Helmholtz free energy density defined in Eq. (3) becomes $W(\lambda_1, \lambda_2, \lambda_3) = 1/2NkT(\lambda_1{}^2 + \lambda_2{}^2 + \lambda_3{}^2 - 3) + \text{const}$ for instantaneous inflation responses. Note that $\lambda_1$, $\lambda_2$, and $\lambda_3$ are defined on the dry state of the hydrogel balloon. To impose the incompressibility condition, let $\Pi$ denote a Lagrange multiplier and add a term $\Pi(J - \hat{J})$ to the free energy density

$$\mathcal{L}(W, \Pi) = W(\lambda_1, \lambda_2, \lambda_3) + \Pi\left(J - \hat{J}\right) \tag{16}$$

The nominal stress in principal directions are

$$S_1 = \frac{\partial \mathcal{L}(W, \Pi)}{\partial \lambda_1} = \frac{\partial W(\lambda_1, \lambda_2, \lambda_3)}{\partial \lambda_1} + \Pi\lambda_2\lambda_3 \tag{17.1}$$

$$S_2 = \frac{\partial \mathcal{L}(W, \Pi)}{\partial \lambda_2} = \frac{\partial W(\lambda_1, \lambda_2, \lambda_3)}{\partial \lambda_2} + \Pi\lambda_1\lambda_3 \tag{17.2}$$

$$S_3 = \frac{\partial \mathcal{L}(W, \Pi)}{\partial \lambda_3} = \frac{\partial W(\lambda_1, \lambda_2, \lambda_3)}{\partial \lambda_3} + \Pi\lambda_1\lambda_2 \tag{17.3}$$

and the principal Cauchy stresses are

$$\sigma_1 = \frac{S_1}{\lambda_2\lambda_3} = \frac{\lambda_1}{\hat{J}}\frac{\partial W(\lambda_1, \lambda_2, \lambda_3)}{\partial \lambda_1} + \Pi \tag{18.1}$$

$$\sigma_2 = \frac{S_2}{\lambda_1\lambda_3} = \frac{\lambda_2}{\hat{J}}\frac{\partial W(\lambda_1, \lambda_2, \lambda_3)}{\partial \lambda_2} + \Pi \tag{18.2}$$

$$\sigma_3 = \frac{S_3}{\lambda_1\lambda_2} = \frac{\lambda_3}{\hat{J}}\frac{\partial W(\lambda_1, \lambda_2, \lambda_3)}{\partial \lambda_3} + \Pi \tag{18.3}$$

For the spherical gel balloon undergoes a spherically symmetric deformation, we have $\sigma_1 = \sigma_2 = \sigma_\theta$, and $\sigma_3 = \sigma_r$, therefore,

$$\sigma_\theta - \sigma_r = \sigma_1 - \sigma_3 = \frac{1}{\hat{J}}\left(\lambda_1\frac{\partial W}{\partial \lambda_1} - \lambda_3\frac{\partial W}{\partial \lambda_3}\right) \tag{19}$$

Insert Eq. (19) into the equation of force balance (Eq. (8)) and integrate from the pressurized inner surface to the stress-free outer surface, we arrive at an expression of the pressure in terms of the deformation of the balloon, i.e., the instantaneous mechanical response to fast inflation

$$\frac{P^{vc}}{kT/v} = 2\frac{H^*}{R^*}\frac{Nv}{\hat{\lambda}}\left[\left(\lambda_\theta^*\right)^{-1} - \left(\lambda_\theta^*\right)^{-7}\right] \tag{20}$$

where $H^* = \hat{\lambda}H$ and $R^* = \hat{\lambda}R$ are the thickness and radius of the hydrogel balloon in the initial isotropic swollen state $S(\hat{C})$ before inflation, $\lambda_\theta^* = \lambda_\theta/\hat{\lambda}$ is defined as the hoop stretch with regard to the reference state $S(\hat{C})$, $P^{vc}$ denotes the applied pressure, and the superscript VC serves as a reminder of the volume-conserving deformation. Note that the pressure-deformation relation depicted by the equation above recovers the well-studied inflation behavior of a balloon made of incompressible Neo-Hookean rubber. By examining the form of Eq. (20), one easily finds that if water migration is not allowed, mechanically the hydrogel behaves as a diluted polymeric material. The equivalent initial shear modulus of such a diluted polymeric network is $Nv/\hat{\lambda}$ (dimensionless). Compared to that of the dry state, the swollen network is softened by a factor of $1/\hat{\lambda}$. Additionally, at $\lambda_\theta^* = 1.383$, the pressure reaches a maximum value of

$$\frac{P_{cr}^{vc}}{kT/v} = 1.24\frac{H^*}{R^*}\frac{Nv}{\hat{\lambda}} \tag{21}$$

This maximum pressure as well constitutes a critical value that the balloon can sustain in a volume-conserving inflation. For $P < P_{cr}^{vc}$, the inflation is steady and the applied pressure carries the balloon to a deformed state that is determined by Eq. (20). Whereas if $P \geq P_{cr}^{vc}$, the balloon grows unstably, leading to a rupture. Since such a failure is not associated with water migration, when the applied load satisfies the failure criterion, it occurs in an instantaneous fashion. Furthermore, Eq. (21) reveals that this critical pressure $P_{cr}^{vc}$ is dependent on the isotropic swelling ratio $\hat{\lambda}$ and thus the water concentration $\hat{C}$: at a specific concentration, there exists a corresponding critical pressure $P_{cr}^{vc}(\hat{C})$ beyond which burst occurs. This conclusion becomes very useful when interpreted equivalently as follows: the criterion to predict whether an instant burst happens or not is whether the applied pressure exceeds $P_{cr}^{vc}(\hat{C})$, which is defined by the water concentration $\hat{C}$ at the current time instance. Particularly, when an inner pressure is suddenly applied to an initially free-swelling hydrogel balloon, the mechanical response of the hydrogel balloon starts with an instantaneous and volume-conserving deformed state. If the load is supercritical, namely, $P \geq P_{cr}^{vc}(C_0)$, the balloon fails instantaneously by burst. We refer to such a failure mechanism as the instant burst of a hydrogel balloon because it takes place immediately upon the pressurization. The instant burst threshold $P_{cr}^{ins}$ of a free-swelling hydrogel balloon is identical to $P_{cr}^{vc}(C_0)$.

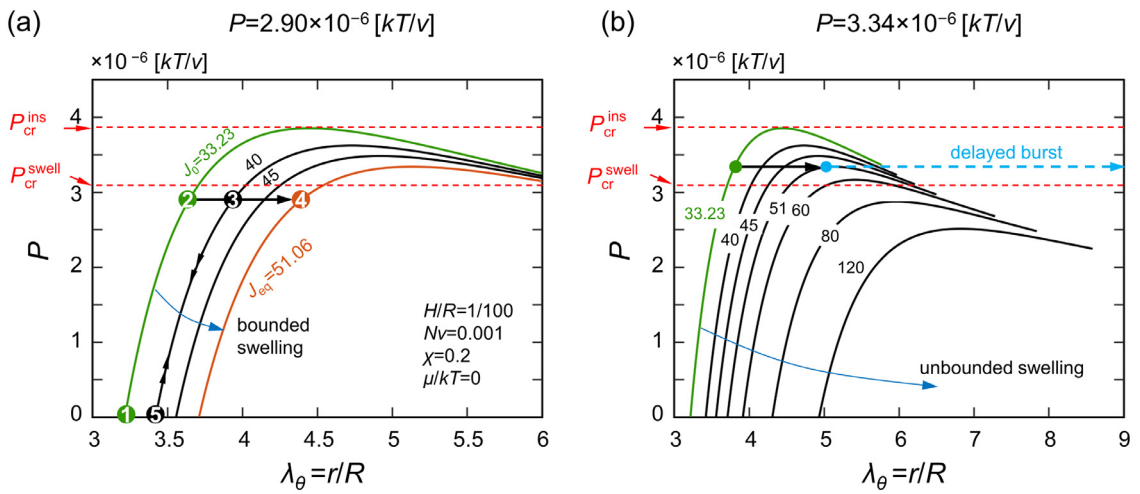


**Fig. 3.** Mechanism of the delayed burst of a hydrogel balloon. (a) Evolution of the intermediate states during inflation when a subcritical pressure of $Pv/kT = 2.90 \times 10^{-6}$ is applied to the balloon. Compared to case (b) when the balloon is subject to a supercritical pressure of $Pv/kT = 3.34 \times 10^{-6}$, delayed burst occurs as a consequence of the unbounded swelling. ②③④ in (a) represents progressively deformed states in response to the applied pressure as the hydrogel shell continues to swell.

Lastly, for hydrogel balloons with different water concentrations, the critical pressure for instant burst is a decreasing function of the homogeneous swelling ratio. According to Eq. (21), the critical pressure is inversely proportional to $\hat{\lambda}$, hence the gel balloon becomes more susceptible to volume-conserving burst if it has more water taken up by the polymeric network. Compare two geometrically identical gel balloons A and B, if $C_A > C_B$, $P_{cr}^{vc}(C_A) < P_{cr}^{vc}(C_B)$.

## 4. Delayed burst of a hydrogel balloon

It is well known that the time-dependent mechanical behavior is one of the most fundamental characteristics of hydrogel materials. The time-dependency may either arise due to the intrinsic viscoelasticity of the constituent cross-linked polymer chains or stem from the poroelasticity that takes accounts for the molecular interaction between the polymer network and the surrounding solvent molecules (Hu and Suo, 2012; Wang and Hong, 2012b). In the present study, we assume the polymer network is ideally elastic and ascribe the time-dependency to the water transportation process through the hydrogel. As aforementioned, mechanical response of a hydrogel subjected to suddenly applied mechanical loads is characterized by an incompressible deformation, followed by a long-term time-dependent deformation towards equilibrium state due to water transportation. In this section, we will systematically study the evolution process of the hydrogel balloon deformation from the instant response state towards the long-term equilibrium state.

When a free-swelling gel balloon is subject to a fast pressurization, even though the water diffusion between the hydrogel and water reservoir is allowed, the immediate response is dominated by the incompressible inflation: if $P \geq P_{cr}^{ins} = P_{cr}^{vc}(C_0)$, instant burst occurs, whereas if $P < P_{cr}^{ins} = P_{cr}^{vc}(C_0)$, the instantaneous deformation is given by Eq. (20) with $\hat{J} = J_0$ and $\hat{\lambda} = \lambda_0$, namely

$$\frac{P}{kT/v} = 2\frac{H}{R}\frac{Nv}{\lambda_0}\left[\left(\lambda_\theta'\right)^{-1} - \left(\lambda_\theta'\right)^{-7}\right] \tag{22}$$

where $\lambda_0$ is the free-swelling stretch ratio sketched in Fig. 1(b) and thus $\lambda_\theta' = \lambda_\theta/\lambda_0$ denotes the hoop stretch relative to the free-swelling state.

However, because of the migration of water molecules, the gel balloon does not stay in this instantaneous deformed state but keeps evolving to equilibrate with the solvent and mechanical loads. Driven by the biaxial stretch state in the hoop directions, the surrounding water molecules in the solvent reservoir start to migrate into the balloon shell. The stiffness of the hydrogel is effectively reduced as the hydrogel balloon swells, which in turn leads to a further expansion under a constant interior pressure. According to Section 2, depending on the applied pressure, subsequent to the instant deformation, the balloon will either arrive at an equilibrium final state through a gradual procedure of simultaneous swelling and expansion, or, in another case, experience an unbounded water intake. For example, if pressure $Pv/kT = 2.90 \times 10^{-6}$ is suddenly pumped into the balloon ($Nv = 0.001$, $H/R = 0.01$), since the load is less than the critical pressure for unbounded swelling $P_{cr}^{swell} v/kT = 3.04 \times 10^{-6}$(see Fig. 2(c) and (d)), eventually the hydrogel balloon will arrive at an equilibrium final state with $\lambda_{eq} = 4.39$ and $J_{eq} = 51.06$, which is determined by solving Eqs. (12) and (13). However, if the hydrogel is subjected to a supercritical pressure $Pv/kT = 3.34 \times 10^{-6}$, the balloon will expand and imbibes water continuously in an unbounded fashion.

The subsequent time-dependent evolution procedure in response to a fast pressurization is explained by Fig. 3. The green curve in Fig. 3(a) plots the incompressible response of the balloon at water content $C_0$ corresponding to the free-

swelling state $\lambda_0 = R_0/R = 3.21$. When a subcritical pressure of $Pv/kT = 2.90 \times 10^{-6}$ is applied, following the green curve, the balloon expands immediately from the initial free-swelling state (denoted by point 1 in Fig. 3(a)) $\lambda_0 = 3.21$ at $J_0 = {\lambda_0}^3 = 33.23$ to the instantaneous deformed state $\lambda_\theta = r/R = 3.64$ at the same volume ratio $J = J_0$ (point 2). During the expansion, the radius grows to 1.13 times of its initial size. Soon afterwards, a small amount of water diffuses into the gel balloon shell, causing the water content to increase to $C_0 + \Delta C$ and the volume ratio to $J_0 + \Delta J$. In response to the water migration, the hydrogel balloon expands further and evolves to a new deformed state, which can be determined by Eq. (20) at the water concentration of $C_0 + \Delta C$. For instance, when water continues to migrate into the gel so that $J = 40$, the deformation of the balloon can be found at the intersection (denoted by point 3) of the volume-conserving response curve with $J = 40$ and the horizontal line $Pv/kT = 2.90 \times 10^{-6}$. Via a sequence of these intervening states, the hydrogel balloon evolves towards its equilibrium final state. Under a constant applied pressure, the state of the hydrogel balloon progresses consecutively across a family of incompressible $P$-$\lambda_\theta$ curves with ascending $J$, from the starting volume ratio $J = J_0$ and terminates at the final equilibrium volume ratio $J_{\text{eq}} = 51.06$ (point 4).

To illustrate that the volume-varying evolution of the gel balloon indeed passes through these intermediate states determined by the family of volume-conversing curves, let us consider an unloading process: at the moment $J = 40$, the boundaries of the gel balloon abruptly loses its permeability, then we drop the pressure. Fully unloaded, the balloon rests at a uniformly swollen state $\lambda_\theta = \lambda_r = 40^{1/3}$ marked by point 5. Lastly, we bring the pressure back to the previous value, the reloading process follows the double arrow from point 5 to point 3 on the incompressible response curve. Therefore, point 5 and 3 is connected by a constant-volume process with $J = 40$, in other words, the intermediate state denoted by point 3 can be identified as the intersection of the incompressible response curve and the applied pressure.

In contrast, if the applied inner pressure is above the critical threshold $P_{\text{cr}}^{\text{swell}} v/kT = 3.04 \times 10^{-6}$, the gel balloon will expand unstably, rather than come to a standstill at a final equilibrium state. Whereas the balloon expands and the hydrogel shell imbibes more water content, the critical pressure for instant burst monotonically decreases as a result of the reduced shear modulus of the diluted polymeric network (Eq. (21)); and the critical pressure for instant burst eventually falls below the applied pressure. As Fig. 3(b) shows, under an applied pressure of $3.34 \times 10^{-6}$, starting from the initial volume ratio $J = J_0 = 33.23$, the hydrogel continuously swells to $J = 51.06$ over time, and the corresponding critical pressure for burst decreases from $P_{\text{cr}}^{\text{ins}} v/kT = P_{\text{cr}}^{\text{vc}}(J = J_0) v/kT = 3.86 \times 10^{-6}$ to the value of the applied pressure, i.e., $3.34 \times 10^{-6}$. As a result, the applied pressure of $3.34 \times 10^{-6}$ triggers the instant burst of the hydrogel balloon when the volume ratio has increased to $J = 51.06$ by water absorption. Compared to the instant failure which occurs immediately upon the pressurization of a free-swelling hydrogel balloon, such burst phenomenon does not take place until a span of time has elapsed after the $Pv/kT = 3.34 \times 10^{-6}$ is applied. The delayed time period is attributed to the time-dependent swelling procedure during which the volume ratio $J$ continuously increases from 33.23 to 51.06 and the critical pressure for instant burst $P_{\text{cr}}^{\text{vc}}(C)$ reduces to the level of the applied pressure $P_{\text{cr}}^{\text{vc}}(C) = P$. The delayed burst of a hydrogel balloon is so named because the onset of it is postponed. Nevertheless, the occurrence of burst itself is instantaneous, as long as the water concentration in the hydrogel shell registers a critical level $C$ such that $P_{\text{cr}}^{\text{vc}}(C) = P$. As analyzed above, unbounded swelling and the decreasing critical pressure $P_{\text{cr}}^{\text{vc}}(C)$ conspire to cause the delayed burst phenomenon. By analogy with the notion of damage mechanics, at a constant pressure load, the capability of the balloon to resist burst failure decays over time as the hydrogel swells, indicating some form of "degradation" is accumulated by virtue of unlimited water migration.

As the delayed burst is a direct consequence of the unbounded swelling, the critical pressure for unbounded swelling $P_{\text{cr}}^{\text{swell}} v/kT = 3.04 \times 10^{-6}$ also defines a critical threshold for delayed burst: when a normalized applied pressure $P < P_{\text{cr}}^{\text{swell}}$, the hydrogel balloon will takes in water and eventually equilibrates with the pressure load and the solvent environment, no burst occurs; whereas if a normalized applied pressure $P_{\text{cr}}^{\text{swell}} \le P < P_{\text{cr}}^{\text{ins}}$ is applied, delayed burst will occur.

The intrinsic time scale of the delayed burst can be estimated by the solvent diffusion dynamics, $t \sim {H_0}^2/D$. At room temperature, diffusivity $D$ can be approximated by the self-diffusivity of water molecules, $D \approx 1 \times 10^{-9}$ m$^2$ s$^{-1}$ (Hong et al., 2008; Wang and Hong, 2012a). For a hydrogel balloon with an initial thickness $H_0 = 1$ mm, the time required by the water molecule to migrate into the balloon shell is on the order of 1000 s, which dictates the characteristic time for the delayed burst. Here, we analyze the delayed burst of a hydrogel balloon by investigating the evolution of the intermediate states from the instant mechanical response of the balloon towards its long-term equilibrium state. A full account of the time-dependent process resorting to directly solving solvent transportation kinetics is beyond the scope of the present paper.

The distinction between equilibrium inflation and delayed burst is also reflected on the free energy landscape. The total free energy of the system is composed of the strain energy of the hydrogel balloon and the potential energy due to the applied pressure. Therefore, the free energy is a function of the applied pressure and the deformation of the balloon

$$\frac{F(J, \lambda_\theta | P)}{\left(\frac{kT}{v}\right) \cdot 4\pi R^3} = \frac{H}{2R} N v \left(2\lambda_\theta^2 + J^2 \lambda_\theta^{-4} - 3 - 2\log J\right) - \frac{H}{R}\left\{\left[(J-1)\log\left(\frac{J}{J-1}\right) + \frac{\chi}{J}\right] + (J-1)\right\} - \frac{1}{3}\frac{P}{\frac{kT}{v}}\lambda_\theta^3 \tag{23}$$

Fig. 4 plots the system free energy in $J$-$\lambda_\theta$ space at (a) a subcritical pressure for delayed burst $Pv/kT = 2.90 \times 10^{-6}$ and (b) a supercritical pressure $3.34 \times 10^{-6}$, respectively. When $Pv/kT = 2.90 \times 10^{-6}$ ($P < P_{\text{cr}}^{\text{swell}}$), as shown in Fig. 4(a), on the free energy surface there exists a local minimum representing the final equilibrium deformation. In the energy contour plot (Fig. 4(a) right panel), the starting point of the white curve denotes the instantaneous deformation state (point 2 in Fig. 3(a)), while the terminal point represents the final equilibrium deformation state (point 4 in Fig. 3(a)). In between, the path connecting the instantaneous response and the final deformation represents the intervening states of the hydrogel balloon. Starting from the instantaneous inflated state, the hydrogel balloon keeps absorbing water with volume ratio $J$

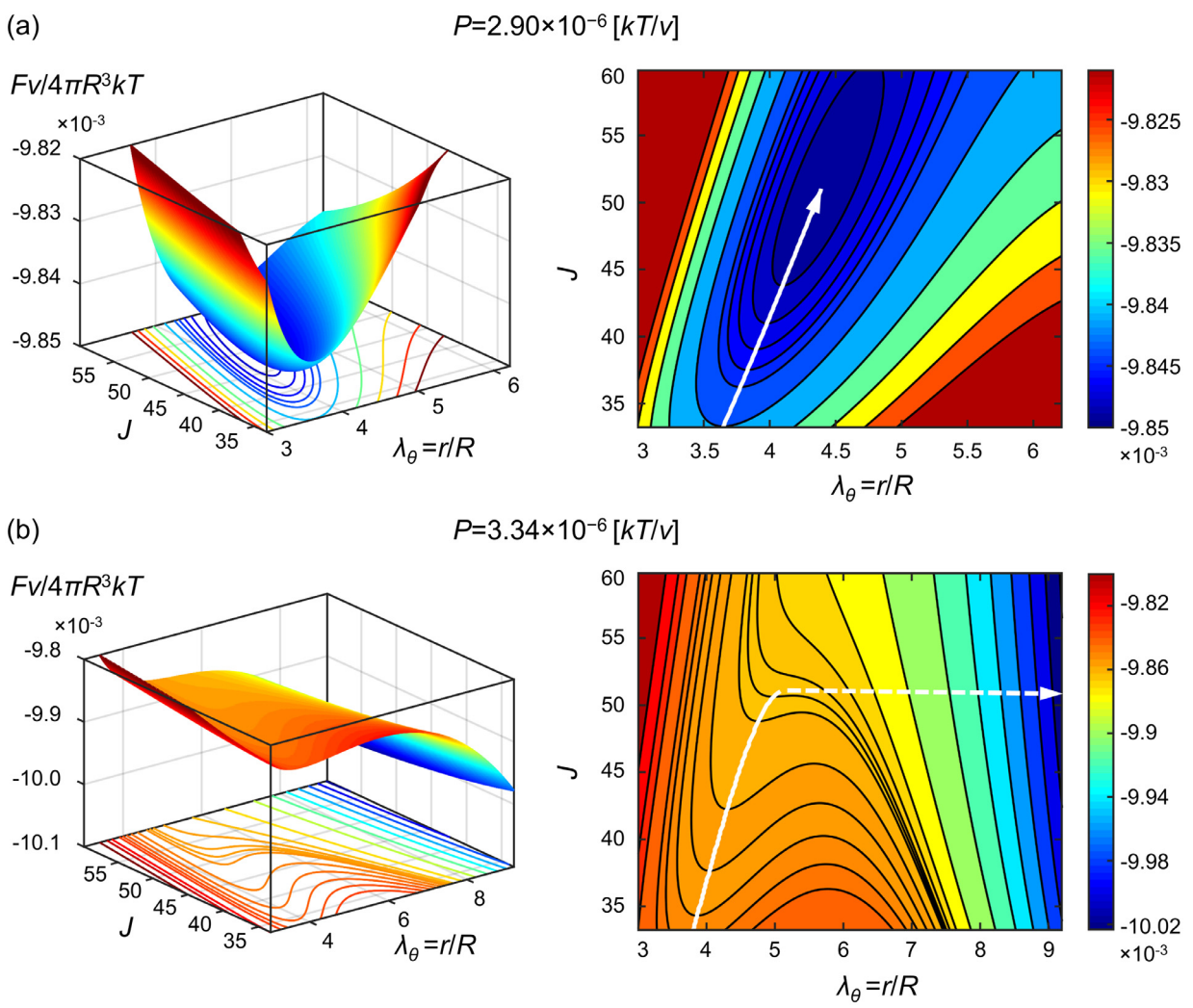


**Fig. 4.** Free energy surface and contour at an applied pressure (a) $Pv/kT = 2.90 \times 10^{-6}$ and (b) $Pv/kT = 3.34 \times 10^{-6}$. The solid white trajectory tracks the minimum energy state of the system as the balloon swells. The white dashed line indicates the delayed burst.

increasing. Since only the water migration requires time whereas the radial expansion of the balloon occurs promptly, at any increased value of $J$, the corresponding hoop stretch $\lambda_\theta = r/R$ should vary to minimize the free energy. The intervening states are thus identified by minimizing the free energy at a given $J$. Consequently, in the $J$-$\lambda_\theta$ space, the inflated hydrogel balloon leaves a white path tracing the evolution of its intermediate states. Driven by the minimization of the total free energy of the system, $= 90 \times$ the balloon continues to swell and expand along the white path until the energy comes to a minimum, and the deformation stops at the final equilibrium state marked by the end of the white arrow.

As shown in Fig. 4(b), the free energy landscape at a supercritical pressure of $Pv/kT = 3.34 \times 10^{-6}$ ($P > P_{cr}^{swell}$) exhibits a lack of local minimum. The first stage of the energy minimization starts from the instantaneous response state at $J = J_0 = 33.23$ (corresponding to the green dot in Fig. 3(b)) to the onset of the delayed burst (end of the white solid line, $J = 51.06$, corresponding to the cyan dot in Fig. 3(b)), during this process the hydrogel balloon slowly absorbs water and grows in size over time. At the turning point where $J = 51.06$, the energy minimum no longer presents, there are actually multiple paths to further minimize the energy. However, the dashed line represents the only way which is not associated with water migration, in other words, it constitutes the fastest path to perform energy minimization that requires no time. Therefore, at $J = 51.06$ the system seeks to minimize the energy by a pure size expansion (burst), as the dashed line indicates.

Furthermore, we can prove that, for an initially free-swelling hydrogel balloon shown in Fig. 1(b), the critical pressure for instant burst $P_{cr}^{ins}$ is always greater than that for delayed burst $P_{cr}^{swell}$, i.e., $P_{cr}^{ins} > P_{cr}^{swell}$ (see Appendix A). For instance, in the previous numerical example, $P_{cr}^{ins} v/kT = 3.86 \times 10^{-6}$ is greater than $P_{cr}^{swell} v/kT = 3.04 \times 10^{-6}$, as shown in Fig. 3(a) and (b). Hence, any applied pressure $P$ may fall into one of three intervals, which are associated with three distinct responses. If $P \geq P_{cr}^{ins}$, the gel balloon bursts immediately upon the load; when $P < P_{cr}^{swell}$, the balloon first deforms to an instantaneous

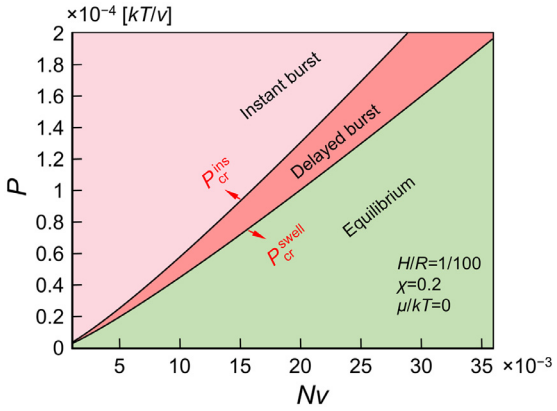


**Fig. 5.** Failure mode map of the inflation of a hydrogel balloon delineating three regions in the parameter space of *P-Nv*: instant burst, delayed burst, and equilibrium inflation.

state then swells and expands further to attain an equilibrium state; if $P_{\mathrm{cr}}^{\mathrm{swell}} \le P < P_{\mathrm{cr}}^{\mathrm{ins}}$, delayed burst occurs, namely the hydrogel balloon expands gradually for a span of time and then bursts suddenly. Fig. 5 delineates a map for these three situations in the parameter space of *P-Nv*. These two pressure limits $P_{\mathrm{cr}}^{\mathrm{ins}}$ and $P_{\mathrm{cr}}^{\mathrm{swell}}$ define the boundary of a new region corresponding to delayed burst failure mode. Owing to its latent nature, such delayed failure mode is more detrimental to the application of thin-walled hydrogel structures.

Recall that the material property $Nv$ represents the crosslinking density and the initial stiffness of the polymer network. Both critical pressures for instant burst $P_{\mathrm{cr}}^{\mathrm{ins}} v/kT$ and for delayed burst $P_{\mathrm{cr}}^{\mathrm{swell}} v/kT$ scale up with stiffness $Nv$. Moreover, as $Nv$ increases, the pressure window associated with the delayed burst becomes larger, because of the increasing difference between $P_{\mathrm{cr}}^{\mathrm{ins}}$ and $P_{\mathrm{cr}}^{\mathrm{swell}}$.

## 5. Delayed burst of a thick hydrogel balloon

In other cases (Dervaux et al., 2011; Hu et al., 2010; Kundu and Crosby, 2009; Mytnyk et al., 2017b; Pan et al., 2016), the thickness of the hollow hydrogel structure may not be essentially small compared to other dimensions, for example, the inner radius of the hollow space. Especially, if the thickness is much larger than the inner radius, the hollow space becomes a cavity defect in a hydrogel. Under pressurization, these structures and defects may be as well susceptible to instant burst and delayed burst. In this section, we investigate the effect of the balloon thickness on the critical pressure for delayed burst.

When the balloon has a finite thickness, the variation of the quantities in the radial direction needs to be accounted for. The stretches $\lambda_\theta$ and $\lambda_{\mathrm{r}}$, water concentration $C$, volume ratio $J$, radial stress $\sigma_{\mathrm{r}}$, and hoop stress $\sigma_\theta$ all vary along the thickness direction. For a special case where the material is incompressible, this boundary value problem represented by Eq. (10) can be integrated analytically,

$$\frac{P^{\mathrm{vc}}}{kT/v} = Nv\left\{\left(\frac{B^3}{B^3-A^3+a^3}\right)^{\frac{1}{3}}\cdot\left[\frac{5B^3-4A^3+4a^3}{2B^3-2A^3+2a^3}\right]-\frac{1}{2}\left(\frac{A}{a}\right)^4-2\frac{A}{a}\right\} \tag{24}$$

where $A$ and $B$ are the inner and outer radii of the hydrogel balloon in the free swelling state (as labeled in Fig. 6(a)), respectively, and $a$ is the inner radius in the deformed state. Before deformation, the thickness of the balloon is $H=B-A$. As previously discussed, if the time scale of interest is much smaller than the characteristic time of the water diffusion, the hydrogel behaves as an incompressible hyperelastic material. Thus, Eq. (24) explicitly gives the response of a thick hydrogel balloon under fast inflation.

Whereas for hyperelastic materials exhibiting compressible behavior, as the quasi-equilibrium deformation during slow pressurization of a hydrogel balloon, the volume-conserving assumption is invalid. Analytical solutions of Eq. (10) are restricted to materials whose constitutive laws take special forms (Ball, 1982; Chung et al., 1986; Horgan, 1992; Podio-Guidugli et al., 1986; Sivaloganathan, 1986) or limited to asymptotic approximations (Dai and Song, 2011). In general, solving the boundary value problem described by Eq. (10) necessitates numerical approaches such as finite difference scheme (for example, shooting method) or alternatively finite element method (FEM) (Lopez-Pamies et al., 2011; Nakamura and Lopez-Pamies, 2012). Here, we examine the slow pressurization procedure by using commercial FEM package ABAQUS. Because the governing equation of the problem Eq. (10) possesses spherical symmetry, it is adequate to merely consider a differential volume that is cut out from the hollow sphere by planes $\Theta=\theta$, $\Theta=\theta+\delta\theta$, $\Phi=\varphi$, $\Phi=\varphi+\delta\varphi$, $\rho=A$, and $\rho=B$, as Fig. 6(a) shows. Note that ABAQUS does not directly supply one-dimensional spherically symmetric element. However, this boundary value problem can be alternatively modeled by using two-dimensional axisymmetric quadrilateral elements under special treat-

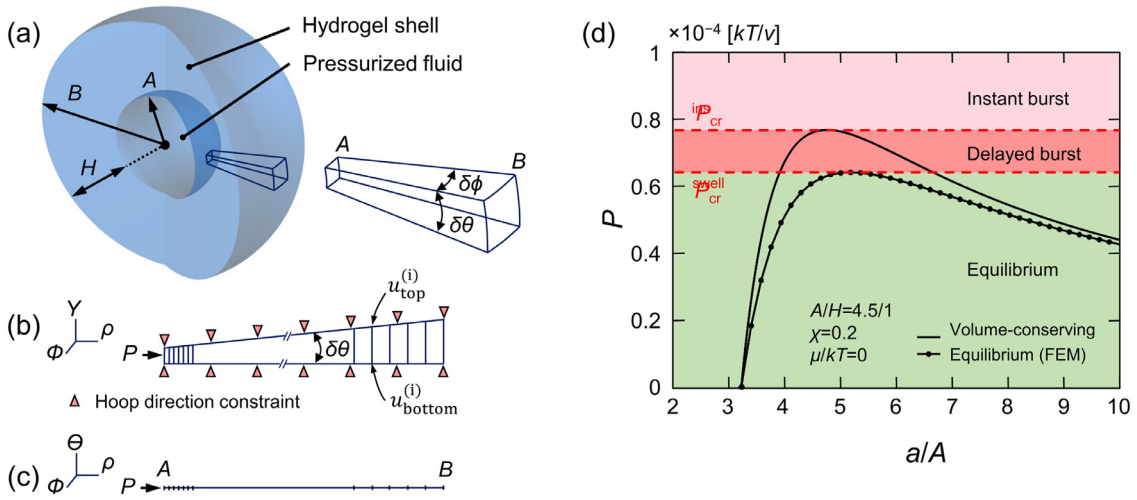


**Fig. 6.** (a) Geometry of a balloon with finite thickness $H = B - A$. $A$ and $B$ are undeformed inner and outer radii, respectively. Schematic of the (b) two-dimensional equivalent FEM representative of the (c) actual one-dimensional model. (d) Normalized pressure $Pv/kT$ as a function of normalized inner surface deformation $a/A$ for instant (volume-conserving) and slow (equilibrium) inflation of a thick balloon. (Hydrogel property $Nv = 0.001$, and balloon geometry $A/H = 4.5/1$).

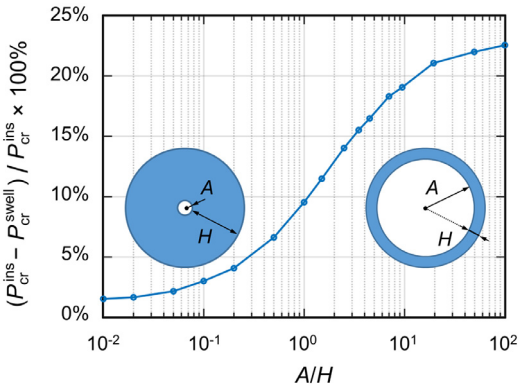


**Fig. 7.** Percentage difference between the critical pressures for instant inflation and unbounded swelling $(P_{cr}^{ins} - P_{cr}^{swell})/P_{cr}^{ins} \times 100\%$, for hydrogel balloons with various thicknesses.

ments that ensure spherically symmetric behavior. Since the integration in one of the hoop directions $\Phi$ is already taken care of by the formation of axisymmetric elements, once we apply suitable boundary conditions to ensure the symmetry in another hoop direction $\Theta$, the spherical symmetry is guaranteed. Therefore, by suppressing the hoop direction freedom, nodes are only free to displace in the radial direction. Furthermore, the radial displacement of nodes on the top side is constrained to be the same as the corresponding nodes on the bottom side, namely $u_{top}^{(i)} = u_{bottom}^{(i)}$, where $(i)$ labels the node number. Now the $\Theta$ direction is discretized by taking advantage of symmetry. Under such a treatment, the two-dimensional model in Fig. 6(b) becomes equivalent to one-dimensional spherically symmetric. In the following analysis, we use $\delta\theta = 0.5$–$1°$. Mesh convergence analysis is also performed in order to ensure the accuracy of the calculation when $A$ is comparatively miniature to $H$. In the next step, equilibrium pressure $P$ is recorded as a function of the prescribed displacement of the inner surface $a$.

Fig. 6(d) compares the final equilibrium deformation to the instant (volume-conserving) response of a thick hydrogel balloon with ratio $A/H = 4.5/1$. The equilibrium inflation response is obtained from FEM, and the instant inflation response is plotted from Eq. (24). Similarly to a thin balloon, the inflation of a thick balloon is also divided into three regions. An applied pressure greater than the peak value of the fast inflation ($P_{cr}^{ins}$) causes instant burst, while a pressure smaller than the maximum pressure on slow inflation curve ($P_{cr}^{swell}$) results in an equilibrium deformation. The peak pressure for fast inflation is higher than that of the slow inflation, carving out a pressure interval for delayed burst to occur.

The predominance of the delayed burst phenomenon can be represented by the difference between the two pressure limits $P_{cr}^{ins}$ and $P_{cr}^{swell}$. Fig. 7 shows the percentage difference $(P_{cr}^{ins} - P_{cr}^{swell})/P_{cr}^{ins} \times 100\%$ for hydrogel balloons with a series of thicknesses from $A/H = 100$ to $A/H = 0.01$. As the thickness increases, the pressure difference is reduced from a highest value of 22% to a minimum value of 2%. The delayed burst phenomenon is more difficult to observe when the wall thickness

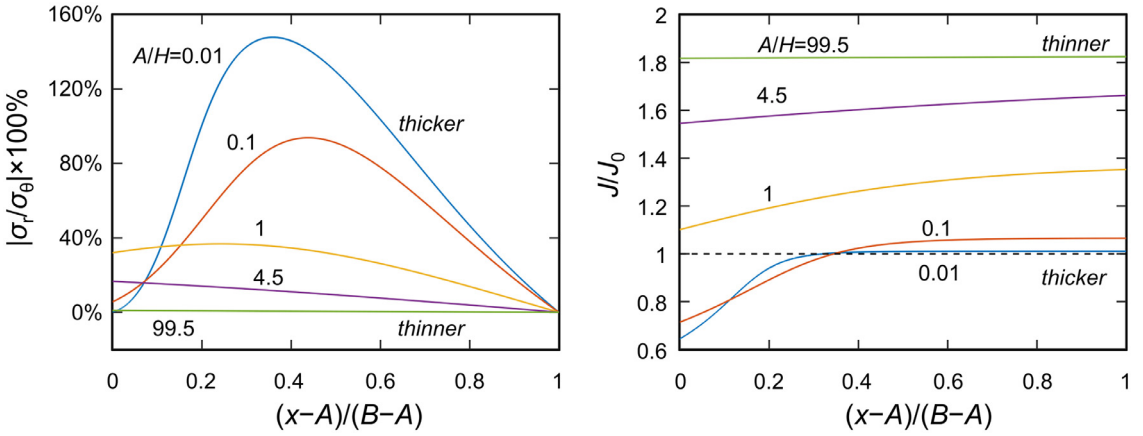


**Fig. 8.** Distribution of (a) stress component ratio $|\sigma_r/\sigma_\theta|$ and (b) relative volume ratio $J/J_0$ at critical pressure $P_{cr}^{swell}$ on equilibrium inflation curve for hydrogel balloons with various thicknesses.

increases. As $A/H$ approaches 0, the critical pressures for instant burst and unbounded swelling tend to merge, and the delayed burst region diminishes on the failure map, indicating that the delayed cavitation becomes less pronounced for an infinitesimal cavity inside the hydrogel body. Ultimately, it might be expected that the importance of delayed burst diminishes as the dimension of inner surface diminishes, and while this is the case, instantaneous failure may become the only prevailing mode of cavitation in hydrogels. The corresponding critical pressure is $2.5Nv$, below which the long-term equilibrium state exists, as predicted by taking the limit of Eq. (24) with $B \gg A$ and $a \gg A$.

In contrast to thin balloons, under inner pressurization, the stress state in a thick balloon deviates from an equal biaxial state. Fig. 8(a) plots the ratio between the radial stress and the hoop stress $|\sigma_r/\sigma_\theta|$ at critical pressure $P_{cr}^{swell}$. As the thickness increases, the radial stress is not negligible anymore when compared with the hoop stress. For a small pressurized cavity inside the hydrogel, between the inner surface and the outer surface, the compressive stress in the radial direction may exceed the tensile stress in the hoop direction. The dissimilarity in the stress states results in distinct distributions of water content and relative volume ratio $J/J_0$. As Fig. 8(b) shows, the water absorption declines as the balloon becomes thicker. In the neighborhood of the inner surface of a small pressurized cavity, the hydrogel even loses water content to the environment. The loss of solvent effectively stiffens the hydrogel, elevates the critical pressure for slow inflation, and consequently, narrows the pressure range for delayed burst or cavitation in a thick hydrogel balloon.

## 6. Conclusion

From the aspect of water migration, this paper investigates the delayed burst phenomenon as a new failure mechanism during the inflation of a hydrogel balloon. In contrast to instantaneous burst, the mechanism of the delayed burst is attributed to an unbounded swelling process subsequent to the instant deformation upon the load. As the hydrogel swells, the instantaneous burst critical pressure of the inflated balloon reduces gradually to the applied inner pressure, triggering the burst. This new failure mode is termed as the delayed burst to signify the fact that the onset of the burst is delayed by a time period for water molecules to migrate into the hydrogel balloon shell. The process of delayed burst is understood by tracking the evolving mechanical response of swelled hydrogel balloon and as well by minimizing the free energy profile of hydrogel balloon subjected to subcritical pressures.

Moreover, we identify the critical pressure for instantaneous burst and delayed burst, along with the three inflation modes of an initially free-swelling hydrogel balloon: If $P \geq P_{cr}^{ins}$, the gel balloon bursts immediately in response to the applied inner pressure; when $P_{cr}^{swell} \leq P < P_{cr}^{ins}$, delayed burst occurs, namely, the hydrogel balloon expands gradually for a span of time and then burst suddenly; if $P < P_{cr}^{swell}$, the balloon first deforms to an instantaneous state upon the load, followed by attaining an equilibrium state via bounded swelling and expansion. We further delineate a map of the three different inflation modes of a thin-walled hydrogel balloon in the parameter space of $P$ and $Nv$: equilibrium inflation ($P < P_{cr}^{swell}$), delayed burst ($P_{cr}^{swell} \leq P < P_{cr}^{ins}$) and instantaneous burst ($P \geq P_{cr}^{ins}$). The delayed burst is counterintuitive and is even more detrimental than the instantaneous burst because of its latent nature.

Lastly, we extend our discussion to examine the delayed burst in thick hydrogel balloons by using finite element method. We find that the delayed burst phenomenon becomes less pronounced for a thick balloon as the pressure window evoking such a failure mode narrows down. Particularly, the delayed cavitation is predicted to become nearly irrelevant for a small vacancy defect enclosed in the hydrogel material. We limit our scope within the geometry of spherical balloons, however, it is believed that this research may also shed light on the delayed failure of other thin-walled hydrogel structures that find extensive applications in soft actuators, soft robots, and biomedical devices.

## Acknowledgments

T. L. and J. C. are grateful for the support of NASA (Grant number: NNX12AM02G). Z. J. acknowledges the financial support from the One-hundred Talents Program of Zhejiang University.

## Appendix A

First, we show that any equilibrium state determined by Eq. (12) is as well located on the incompressible response curve. For an arbitrary equilibrium state of the balloon, let us denote the volume ratio as

$$J = \hat{J} = \hat{\lambda}^3 \tag{A1}$$

inserting Eq. (23) into Eq. (12) gives,

$$\frac{P}{kT/v} = \frac{2H}{R} N\nu \cdot \left(\lambda_\theta^{-1} - \lambda_\theta^{-7}\hat{\lambda}^6\right) = \frac{2\left(\hat{\lambda}H\right)}{\left(\hat{\lambda}R\right)} \frac{N\nu}{\hat{\lambda}} \left( \left(\frac{\lambda_\theta}{\hat{\lambda}}\right)^{-1} - \left(\frac{\lambda_\theta}{\hat{\lambda}}\right)^{-7} \right) \tag{A2}$$

which recovers Eq. (20), namely the instantaneous response of a hydrogel balloon at a uniform initial swelling ratio $\hat{\lambda}$. Therefore, we have proved that any equilibrium state can also be achieved through a volume-conserving process at the corresponding volume ratio $J$. Among all these equilibrium states, the critical pressure for unbounded swelling $P_{\mathrm{cr}}^{\mathrm{swell}}$ corresponds to a specific one, which is the equilibrium state at the highest water content $J$ or the highest volume ratio $C$.

As $J$ increases from $J_0$ to $J_{\mathrm{eq}}$, the critical pressure for instant burst at the initial free-swelling state $P_{\mathrm{cr}}^{\mathrm{ins}}$ is actually the highest pressure on all the instant response curves at different values of $J$. Therefore, the critical pressure for instant burst $P_{\mathrm{cr}}^{\mathrm{ins}}$ is always greater than that for the unbounded swelling, i.e., $P_{\mathrm{cr}}^{\mathrm{ins}} > P_{\mathrm{cr}}^{\mathrm{swell}}$.

## References

Acome, E., Mitchell, S.K., Morrissey, T.G., Emmett, M.B., Benjamin, C., King, M., Radakovitz, M., Keplinger, C., 2018. Hydraulically amplified self-healing electrostatic actuators with muscle-like performance. Science 359, 61–65. https://doi.org/10.1126/science.aao6139.

Ainla, A., Verma, M.S., Yang, D., Whitesides, G.M., 2017. Soft, rotating pneumatic actuator. Soft Robot. 4, 297–304. https://doi.org/10.1089/soro.2017.0017.

Alessandri, K., Sarangi, B.R., Gurchenkov, V.V., Sinha, B., Kießling, T.R., Fetler, L., Rico, F., Scheuring, S., Lamaze, C., Simon, A., Geraldo, S., Vignjevic, D., Doméjean, H., Rolland, L., Funfak, A., Bibette, J., Bremond, N., Nassoy, P., 2013. Cellular capsules as a tool for multicellular spheroid production and for investigating the mechanics of tumor progression in vitro. Proc. Natl. Acad. Sci. USA. 110, 14843–14848. https://doi.org/10.1073/pnas.1309482110.

Alexander, H., 1971. Tensile instability of initially spherical balloons. Int. J. Eng. Sci. 9, 151–160. https://doi.org/10.1016/0020-7225(71)90017-6.

Alijotas-Reig, J., Fernández-Figueras, M.T., Puig, L., 2013. Late-onset inflammatory adverse reactions related to soft tissue filler injections. Clin. Rev. Allergy Immunol. 45, 97–108. https://doi.org/10.1007/s12016-012-8348-5.

Ball, J.M., 1982. Discontinuous equilibrium solutions and cavitation in nonlinear elasticity. Philos. Trans. R. Soc. A Math. Phys. Eng. Sci. 306, 557–611. https://doi.org/10.1098/rsta.1982.0095.

Bartlett, N.W., Tolley, M.T., Overvelde, J.T.B., Weaver, J.C., Mosadegh, B., Bertoldi, K., Whitesides, G.M., Wood, R.J., 2015. A 3D-printed, functionally graded soft robot powered by combustion. Science 349, 161–165. https://doi.org/10.1126/science.aab0129.

Baumberger, T., Caroli, C., Martina, D., 2006. Solvent control of crack dynamics in a reversible hydrogel. Nat. Mater. 5, 552–555. https://doi.org/10.1038/nmat1666.

Bertrand, T., Peixinho, J., Mukhopadhyay, S., MacMinn, C.W., 2016. Dynamics of swelling and drying in a spherical gel. Phys. Rev. Appl. 6, 064010. https://doi.org/10.1103/PhysRevApplied.6.064010.

Bogen, D.K., McMahon, T.A., 1979. Do cardiac aneurysms blow out? Biophys. J. 27, 301–316. https://doi.org/10.1016/S0006-3495(79)85219-4.

Bonn, D., Kellay, H., Prochnow, M., Ben-Djemiaa, K., Meunier, J., 1998. Delayed fracture of an inhomogeneous soft solid. Science 280, 265–267. https://doi.org/10.1126/SCIENCE.280.5361.265.

Chaudhury, M.K., 1999. Rate-dependent fracture at adhesive interface. J. Phys. Chem. B 103, 6562–6566. https://doi.org/10.1021/JP9906482.

Chen, Y., Healey, T.J., 1991. Bifurcation to pear-shaped equilibria of pressurized spherical membranes. Int. J. NonLinear Mech. 26, 279–291. https://doi.org/10.1016/0020-7462(91)90058-2.

Chung, D.-T., Horgan, C.O., Abeyaratne, R., 1986. The finite deformation of internally pressurized hollow cylinders and spheres for a class of compressible elastic materials. Int. J. Solids Struct. 22, 1557–1570. https://doi.org/10.1016/0020-7683(86)90062-4.

Curatolo, M., Nardinocchi, P., Puntel, E., Teresi, L., 2017. Transient instabilities in the swelling dynamics of a hydrogel sphere. J. Appl. Phys. 122, 145109. https://doi.org/10.1063/1.5007229.

Dai, H.-H., Song, Z., 2011. Some analytical formulas for the equilibrium states of a swollen hydrogel shell. Soft Matter 7, 8473. https://doi.org/10.1039/c1sm05425b.

deBotton, G., Bustamante, R., Dorfmann, A., 2013. Axisymmetric bifurcations of thick spherical shells under inflation and compression. Int. J. Solids Struct. 50, 403–413. https://doi.org/10.1016/J.IJSOLSTR.2012.10.004.

Dervaux, J., Couder, Y., Guedeau-Boudeville, M.-A., Ben Amar, M., 2011. Shape transition in artificial tumors: from smooth buckles to singular creases. Phys. Rev. Lett. 107, 018103. https://doi.org/10.1103/PhysRevLett.107.018103.

Feodos'ev, V.I., 1968. On equilibrium modes of a rubber spherical shell under internal pressure. J. Appl. Math. Mech. 32, 339–344. https://doi.org/10.1016/0021-8928(68)90138-X.

Fujine, M., Takigawa, T., Urayama, K., 2015. Strain-driven swelling and accompanying stress reduction in polymer gels under biaxial stretching. Macromolecules 48, 3622–3628. https://doi.org/10.1021/acs.macromol.5b00642.

Godoy, L.A., 2016. Buckling of vertical oil storage steel tanks: Review of static buckling studies. Thin-Walled Struct. 103, 1–21. https://doi.org/10.1016/J.TWS.2016.01.026.

Griffin, D.R., Weaver, W.M., Scumpia, P.O., Di Carlo, D., Segura, T., 2015. Accelerated wound healing by injectable microporous gel scaffolds assembled from annealed building blocks. Nat. Mater. 14, 737–744. https://doi.org/10.1038/nmat4294.

Hong, W., Liu, Z., Suo, Z., 2009. Inhomogeneous swelling of a gel in equilibrium with a solvent and mechanical load. Int. J. Solids Struct. 46, 3282–3289. https://doi.org/10.1016/J.IJSOLSTR.2009.04.022.

Hong, W., Zhao, X., Zhou, J., Suo, Z., 2008. A theory of coupled diffusion and large deformation in polymeric gels. J. Mech. Phys. Solids 56, 1779–1793. https://doi.org/10.1016/j.jmps.2007.11.010.

Horgan, C.O., 1992. Void nucleation and growth for compressible non-linearly elastic materials: an example. Int. J. Solids Struct. 29, 279–291. https://doi.org/10.1016/0020-7683(92)90200-D.
Hu, X., Tong, Z., Lyon, L.A., 2010. Multicompartment core/shell microgels. J. Am. Chem. Soc. 132, 11470–11472. https://doi.org/10.1021/ja105616v.
Hu, Y., Suo, Z., 2012. Viscoelasticity and poroelasticity in elastomeric gels. Acta Mech. Solida Sin. 25, 441–458. https://doi.org/10.1016/S0894-9166(12)60039-1.
Kim, D.-H., Lu, N., Ghaffari, R., Kim, Y.-S., Lee, S.P., Xu, L., Wu, J., Kim, R.-H., Song, J., Liu, Z., Viventi, J., de Graff, B., Elolampi, B., Mansour, M., Slepian, M.J., Hwang, S., Moss, J.D., Won, S.-M., Huang, Y., Litt, B., Rogers, J.A., 2011. Materials for multifunctional balloon catheters with capabilities in cardiac electrophysiological mapping and ablation therapy. Nat. Mater. 10, 316–323. https://doi.org/10.1038/nmat2971.
Kundu, S., Crosby, A.J., 2009. Cavitation and fracture behavior of polyacrylamide hydrogels. Soft Matter 5, 3963. https://doi.org/10.1039/b909237d.
Lee, A., López Jiménez, F., Marthelot, J., Hutchinson, J.W., Reis, P.M., 2016. The geometric role of precisely engineered imperfections on the critical buckling load of spherical elastic shells. J. Appl. Mech. 83, 111005. https://doi.org/10.1115/1.4034431.
Li, J., Mooney, D.J., 2016. Designing hydrogels for controlled drug delivery. Nat. Rev. Mater.. https://doi.org/10.1038/natrevmats.2016.71.
Li, T., Keplinger, C., Baumgartner, R., Bauer, S., Yang, W., Suo, Z., 2013. Giant voltage-induced deformation in dielectric elastomers near the verge of snap-through instability. J. Mech. Phys. Solids 61, 611–628. https://doi.org/10.1016/J.JMPS.2012.09.006.
Lima, A.C., Batista, P., Valente, T.A.M., Silva, A.S., Correia, I.J., Mano, J.F., 2013. Novel methodology based on biomimetic superhydrophobic substrates to immobilize cells and proteins in hydrogel spheres for applications in bone regeneration. Tissue Eng. Part A 19, 1175–1187. https://doi.org/10.1089/ten.tea.2012.0249.
Lindström, S.B., Kodger, T.E., Sprakel, J., Weitz, D.A., 2012. Structures, stresses, and fluctuations in the delayed failure of colloidal gels. Soft Matter 8, 3657. https://doi.org/10.1039/c2sm06723d.
Lopez-Pamies, O., Nakamura, T., Idiart, M.I., 2011. Cavitation in elastomeric solids: II—onset-of-cavitation surfaces for Neo-Hookean materials. J. Mech. Phys. Solids 59, 1488–1505. https://doi.org/10.1016/J.JMPS.2011.04.016.
Lu, T., An, L., Li, J., Yuan, C., Wang, T.J., 2015. Electro-mechanical coupling bifurcation and bulging propagation in a cylindrical dielectric elastomer tube. J. Mech. Phys. Solids 85, 160–175. https://doi.org/10.1016/J.JMPS.2015.09.010.
Lu, Y., Song, W., An, D., Kim, B.J., Schwartz, R., Wu, M., Ma, M., 2015. Designing compartmentalized hydrogel microparticles for cell encapsulation and scalable 3D cell culture. J. Mater. Chem. B 3, 353–360. https://doi.org/10.1039/C4TB01735H.
Luo, R., Cao, Y., Shi, P., Chen, C.-H., 2014. Near-infrared light responsive multi-compartmental hydrogel particles synthesized through droplets assembly induced by superhydrophobic surface. Small 10, 4886–4894. https://doi.org/10.1002/smll.201401312.
Mao, Y., Anand, L., 2018. A theory for fracture of polymeric gels. J. Mech. Phys. Solids 115, 30–53. https://doi.org/10.1016/J.JMPS.2018.02.008.
Marchese, A.D., Onal, C.D., Rus, D., 2014. Autonomous soft robotic fish capable of escape maneuvers using fluidic elastomer actuators. Soft Robot. 1, 75–87. https://doi.org/10.1089/soro.2013.0009.
Marthelot, J., López Jiménez, F., Lee, A., Hutchinson, J.W., Reis, P.M., 2017. Buckling of a pressurized hemispherical shell subjected to a probing force. J. Appl. Mech. 84, 121005. https://doi.org/10.1115/1.4038063.
Merritt, D.R., Weinhaus, F., 1978. The pressure curve for a rubber balloon. Am. J. Phys. 46, 976–977. https://doi.org/10.1119/1.11486.
Mytnyk, S., Ziemecka, I., Olive, A.G.L., van der Meer, J.W.M., Totlani, K.A., Oldenhof, S., Kreutzer, M.T., van Steijn, V., van Esch, J.H., 2017a. Microcapsules with a permeable hydrogel shell and an aqueous core continuously produced in a 3D microdevice by all-aqueous microfluidics. RSC Adv. 7, 11331–11337. https://doi.org/10.1039/C7RA00452D.
Mytnyk, S., Ziemecka, I., Olive, A.G.L., van der Meer, J.W.M., Totlani, K.A., Oldenhof, S., Kreutzer, M.T., van Steijn, V., van Esch, J.H., 2017b. Microcapsules with a permeable hydrogel shell and an aqueous core continuously produced in a 3D microdevice by all-aqueous microfluidics. RSC Adv. 7, 11331–11337. https://doi.org/10.1039/C7RA00452D.
Nakamura, T., Lopez-Pamies, O., 2012. A finite element approach to study cavitation instabilities in non-linear elastic solids under general loading conditions. Int. J. NonLinear Mech. 47, 331–340. https://doi.org/10.1016/J.IJNONLINMEC.2011.07.007.
Needleman, A., 1977. Inflation of spherical rubber balloons. Int. J. Solids Struct. 13, 409–421. https://doi.org/10.1016/0020-7683(77)90036-1.
Nemiroski, A., Shevchenko, Y.Y., Stokes, A.A., Unal, B., Ainla, A., Albert, S., Compton, G., MacDonald, E., Schwab, Y., Zellhofer, C., Whitesides, G.M., 2017. Arthrobots. Soft Robot.. soro.2016.0043 https://doi.org/10.1089/soro.2016.0043 .
Olabisi, R.M., Lazard, Z.W., Franco, C.L., Hall, M.A., Kwon, S.K., Sevick-Muraca, E.M., Hipp, J.A., Davis, A.R., Olmsted-Davis, E.A., West, J.L., 2010. Hydrogel microsphere encapsulation of a cell-based gene therapy system increases cell survival of injected cells, transgene expression, and bone volume in a model of heterotopic ossification. Tissue Eng. Part A 16, 3727–3736. https://doi.org/10.1089/ten.tea.2010.0234.
Overvelde, J.T.B., Kloek, T., D'haen, J.J.A., Bertoldi, K., 2015. Amplifying the response of soft actuators by harnessing snap-through instabilities. Proc. Natl. Acad. Sci. USA. 112, 10863–10868. https://doi.org/10.1073/pnas.1504947112.
Pan, H.M., Seuss, M., Neubauer, M.P., Trau, D.W., Fery, A., 2016. Tuning the mechanical properties of hydrogel core–shell particles by inwards interweaving self-assembly. ACS Appl. Mater. Interfaces 8, 1493–1500. https://doi.org/10.1021/acsami.5b10886.
Podio-Guidugli, P., Caffarelli, G.V., Virga, E.G., 1986. Discontinuous energy minimizers in nonlinear elastostatics: an example of J. Ball revisited. J. Elast. 16, 75–96. https://doi.org/10.1007/BF00041067.
Scherer, G.W., Smith, D.M., 1995. Cavitation during drying of a gel. J. Non Cryst. Solids 189, 197–211. https://doi.org/10.1016/0022-3093(95)00222-7.
Shepherd, R.F., Ilievski, F., Choi, W., Morin, S.A., Stokes, A.A., Mazzeo, A.D., Chen, X., Wang, M., Whitesides, G.M., 2011. Multigait soft robot. Proc. Natl. Acad. Sci. USA. 108, 20400–20403. https://doi.org/10.1073/pnas.1116564108.
Sivaloganathan, J., 1986. Uniqueness of regular and singular equilibria for spherically symmetric problems of nonlinear elasticity. Arch. Ration. Mech. Anal. 96, 97–136. https://doi.org/10.1007/BF00251407.
Skrzeszewska, P.J., Sprakel, J., de Wolf, F.A., Fokkink, R., Cohen Stuart, M.A., van der Gucht, J., 2010. Fracture and self-healing in a well-defined self-assembled polymer network. Macromolecules 43, 3542–3548. https://doi.org/10.1021/ma1000173.
Song, W., Lu, Y., Frankel, A.S., An, D., Schwartz, R.E., Ma, M., 2015. Engraftment of human induced pluripotent stem cell-derived hepatocytes in immunocompetent mice via 3D co-aggregation and encapsulation. Sci. Rep. 5, 16884. https://doi.org/10.1038/srep16884.
Tang, J., Li, J., Vlassak, J.J., Suo, Z., 2017. Fatigue fracture of hydrogels. Extreme Mech. Lett. 10, 24–31. https://doi.org/10.1016/J.EML.2016.09.010.
Wang, F., Yuan, C., Lu, T., Wang, T.J., 2017. Anomalous bulging behaviors of a dielectric elastomer balloon under internal pressure and electric actuation. J. Mech. Phys. Solids 102, 1–16. https://doi.org/10.1016/J.JMPS.2017.01.021.
Wang, H., Cai, S., 2015a. Drying-induced cavitation in a constrained hydrogel. Soft Matter 11, 1058–1061. https://doi.org/10.1039/C4SM02652G.
Wang, H., Cai, S., 2015b. Cavitation in a swollen elastomer constrained by a non-swellable shell. J. Appl. Phys. 117, 154901. https://doi.org/10.1063/1.4918278.
Wang, X., Hong, W., 2012a. Delayed fracture in gels. Soft Matter 8, 8171–8178. https://doi.org/10.1039/c2sm25553g.
Wang, X., Hong, W., 2012b. A visco-poroelastic theory for polymeric gels. Proc. R. Soc. A Math. Phys. Eng. Sci. 468, 3824–3841. https://doi.org/10.1098/rspa.2012.0385.
Wang, Y., Wang, J., 2014. Mixed hydrogel bead-based tumor spheroid formation and anticancer drug testing. Analyst 139, 2449–2458. https://doi.org/10.1039/C4AN00015C.
Wehner, M., Truby, R.L., Fitzgerald, D.J., Mosadegh, B., Whitesides, G.M., Lewis, J.A., Wood, R.J., 2016. An integrated design and fabrication strategy for entirely soft, autonomous robots. Nature 536, 451–455. https://doi.org/10.1038/nature19100.
Yao, Y., McDowell, M.T., Ryu, I., Wu, H., Liu, N., Hu, L., Nix, W.D., Cui, Y., 2011. Interconnected silicon hollow nanospheres for lithium-ion battery anodes with long cycle life. Nano Lett 11, 2949–2954. https://doi.org/10.1021/nl201470j.
Yoshida, K., Onoe, H., 2017. Functionalized core-shell hydrogel microsprings by anisotropic gelation with bevel-tip capillary. Sci. Rep. 7, 45987. https://doi.org/10.1038/srep45987.

Yuk, H., Lin, S., Ma, C., Takaffoli, M., Fang, N.X., Zhao, X., 2017. Hydraulic hydrogel actuators and robots optically and sonically camouflaged in water. Nat. Commun. 8, 14230. https://doi.org/10.1038/ncomms14230.

Zamani, V., Pence, T.J., 2017. Swelling, inflation, and a swelling-burst instability in hyperelastic spherical shells. Int. J. Solids Struct. 125, 134–149. https://doi.org/10.1016/J.IJSOLSTR.2017.07.010.

Zhao, S., Agarwal, P., Rao, W., Huang, H., Zhang, R., Liu, Z., Yu, J., Weisleder, N., Zhang, W., He, X., 2014. Coaxial electrospray of liquid core–hydrogel shell microcapsules for encapsulation and miniaturized 3D culture of pluripotent stem cells. Integr. Biol. 6, 874–884. https://doi.org/10.1039/C4IB00100A.